Iterative solution of the electromagnetic inverse scattering problem from the transient scattered field

André Dubois, K. Belkebir, Ilaria Catapano, Marc Saillard

Iterative solution of the electromagnetic inverse scattering problem from the transient scattered field

A. Dubois,[1] K. Belkebir,[2] I. Catapano,[3] and M. Saillard[4]

Received 30 October 2007; revised 21 August 2008; accepted 15 December 2008; published 14 February 2009.

[1] This paper deals with an iterative approach to solve the electromagnetic inverse scattering problem from single view transient data. The measurement configuration consists in illuminating a two-dimensional scattering system with an electromagnetic transient source and in measuring the time domain response all around the investigated region. The aim is then to determine the electromagnetic properties of the target from the measurements. The problem is formulated in the frequency domain for a large number of frequencies, such that the incident pulse is accurately sampled, rather than in the time domain. The parameters of interest, namely, the relative permittivity and the conductivity profiles, are built up iteratively by minimizing a cost functional involving the discrepancy between the measured scattered fields and those that would be obtained via a forward model. Numerical examples are presented to prove the efficiency of the suggested method and its robustness against noise. The influence of the central frequency and of the bandwidth of the incident field on the achievable performances is also illustrated.

Citation: Dubois, A., K. Belkebir, I. Catapano, and M. Saillard (2009), Iterative solution of the electromagnetic inverse scattering problem from the transient scattered field, *Radio Sci.*, *44*, RS1007, doi:10.1029/2007RS003765.

1. Introduction

[2] Inverse scattering problems play an important role in many applications, which require a non invasive characterization of unknown objects. These applications bring different areas together, like geophysical probing, medical imaging or nondestructive evaluation. The aim of inverse problems is to retrieve the features (i.e., position, geometry and constitutive materials) of unknown targets from the knowledge of their scattered fields.

[3] The most popular strategy for solving this ill-posed and nonlinear problem is to reconstruct the parameters of interest iteratively, by minimizing a cost functional involving the discrepancy between the data and the scattered fields that would be obtained via a forward model from the best available estimation of the parameter. In the frequency domain, a theoretical analysis of the dynamic range as well as of the spatial resolution of linearized schemes [*Tijhuis et al.*, 2001a] shows that the convergence is better at low frequencies, with however a ''poor'' resolution, while at higher frequencies the resolution is improved but the convergence is not guaranteed.

[4] To circumvent the foreseen difficulties, a multiple frequency approach, known as frequency-hopping approach [*Chew and Lin*, 1995] has been proposed. In this approach, the iterative inversion process starts at low frequencies in order to get a trend that is used as an initial guess for the inversion at higher frequencies, thus making possible to retrieve the object under test with high resolution. Successful results have been obtained from synthetic data [*Tijhuis et al.*, 2001a] as well as experimental data [*Tijhuis et al.*, 2001b].

[5] Another way to overcome these difficulties is to use transient data. In this case, targets are illuminated by a short time duration pulse, that is to say a wideband incident field, so that both low frequencies, required to ensure convergence of the algorithm, and high frequencies, which improve the spatial resolution, are considered at the same time in the inversion scheme.

[6] The inversion of transient fields may also be tackled in two ways depending on the formulation of

[1] LIST, CEA, Gif-sur-Yvette, France.
[2] Institut Fresnel, UMR6133, Universités d'Aix-Marseille I and III, CNRS, Marseille, France.
[3] Institute for Electromagnetic Sensing of the Environment, IREA-CNR, Naples, Italy.
[4] LSEET, UMR6017, Université de Sud Toulon-Var, CNRS, La Garde, France.

0048-6604/09/2007RS003765

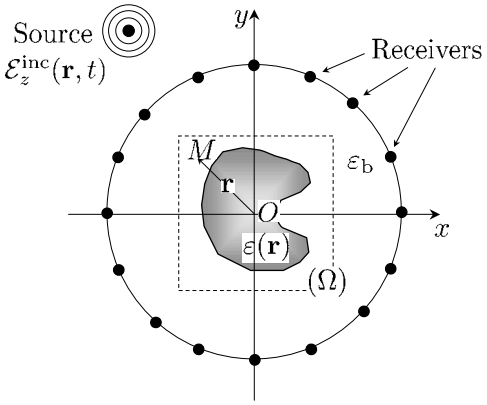

Figure 1. Geometry of the problem. The target under test is assumed to be confined in a bounded box Ω and illuminated by an electromagnetic source radiating a transient field.

the scattering problem, either in the frequency domain [*Moghaddam and Chew*, 1992, 1993] or directly in the time domain [*Tijhuis*, 1981; *Weedon and Chew*, 1993]. In the present work, the first representation has been preferred because it has some advantages like the restriction of the computational domain to the scattering domain, boundaries conditions inherently satisfied through the appropriate Green function and possibility to take easily into account the dispersion of the background media as well as the target under test, etc. The main bottleneck solving the transient scattering problem in the frequency domain is that repeated field computations require an excessive amount of computation time. However, the computational time may be reduced drastically by using a special extrapolation procedure as suggested by *Peng and Tijhuis* [1993] and *Tijhuis et al.* [2001a]. Therefore Maxwell's equations as well as data are expressed in the frequency domain thanks to a temporal Fourier transform. This allows us to investigate two different strategies. The first one is the frequency hopping in which inversions are performed sequentially starting from low frequencies and using final results as initial guesses for inversion at higher frequencies. In the second approach, inversion of transient data, entire spectra of data are inverted once. This paper is restricted to two-dimensional targets embedded in a homogeneous background.

2. Statement of the Problem

[7] The geometry of the scattering problem under study is described in Figure 1. A two-dimensional target, with arbitrary cross section confined in a bounded domain, the investigated region Ω, is embedded in an infinite and homogeneous medium of complex permittivity $\tilde{\varepsilon}_b = \varepsilon_0 \tilde{\varepsilon}_{rb}(\omega)$, ε_0 and $\tilde{\varepsilon}_{rb}$ being the permittivity of vacuum and the relative permittivity of the background at the angular frequency ω, respectively. Scatterers are assumed to be inhomogeneous cylinders of complex permittivity $\tilde{\varepsilon}(\mathbf{r}, \omega) = \varepsilon_0 \tilde{\varepsilon}_r(\mathbf{r}, \omega)$. All materials are nonmagnetic ($\mu = \mu_0$, everywhere).

[8] A right-handed Cartesian coordinate frame (O, $\mathbf{u}_x$, $\mathbf{u}_y$, $\mathbf{u}_z$) is defined, with z axis parallel to the direction of invariance. The position of a point M is given by:

$$\mathbf{OM} = x\mathbf{u}_x + y\mathbf{u}_y + z\mathbf{u}_z = \mathbf{r} + z\mathbf{u}_z. \qquad (1)$$

The investigated region is illuminated by a line source parallel to the z axis and fed by a current $\mathcal{I}(t)$, thus generating a transient incident field $\mathcal{E}^{\mathrm{inc}}(\mathbf{r}, t)$. A short Gaussian pulse is used, leading to a bandwidth to central frequency ratio $\Delta f/f_0 \simeq 0.5$, as shown in Figure 2. The scattered field is measured by N_r receivers located on a line Γ surrounding the target. The study is restricted to

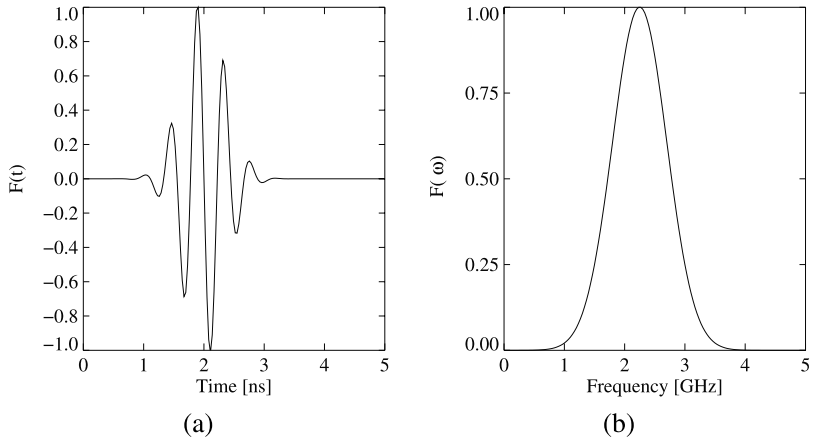

Figure 2. Shape of the incident field: (a) in the time domain, (b) modulus of its Fourier transform.

the transverse magnetic (TM) polarization case. Therefore only the z component of the involved electrical fields is considered.

[9] By taking into account the Parseval theorem, the inverse scattering problem can be formulated in the frequency domain rather then in the time domain, provided that the transient fields are replaced by the corresponding time-harmonic ones and the involved frequency range is sampled according to Shannon's theorem. However, this may lead to consider a large and redundant number L of time harmonics problems. As discussed by *Bucci et al.* [2000], the use of multifrequency data (instead of monochromatic ones) offers the possibility to enlarge the amount of available independent information and then to improve the local stability and robustness against false solutions of the inverse approach. On the other hand, recording the data at two different frequencies does not means to double up the amount of independent information, while it certainly leads to increase the processing times required by the inversion procedure. Then, a key issue is to understand how many frequencies have to be considered in a given frequency range in order to improve the achievable performances, while keeping acceptable the computational effort. Some useful advises on this point are given by *Bucci et al.* [2000] and *Catapano et al.* [2006]. Let us define the time Fourier transform as:

$$E(\mathbf{r},\omega)=\int_{-\infty}^{+\infty}\exp(\mathrm{i}\omega t)\mathcal{E}(\mathbf{r},t)\mathrm{d}t, \tag{2}$$

$E(\mathbf{r}, \omega)$ is discretized with respect to frequency into L components and lth frequency component of $E(\mathbf{r}, \omega)$ is from now on denoted as $E_l(\mathbf{r})$.

[10] The electromagnetic scattering problem can then be formulated, for each frequency f_l, with $l = 1, \cdots, L$, as two coupled contrast-source equations. The observation equation (equation (3)) expresses the scattered field E_l^{d} at $\mathbf{r}$ on Γ and the state equation (equation (4)) expresses the total field in Ω.

$$E_l^{\mathrm{d}}(\mathbf{r}\in\Gamma)=k_{0,l}^2\int_{\Omega}\chi_l(\mathbf{r}')E_l(\mathbf{r}')G_{l,\Gamma}(\mathbf{r},\mathbf{r}')\mathrm{d}\mathbf{r}'. \tag{3}$$

$$E_l(\mathbf{r}\in\Omega)=E_l^{\mathrm{inc}}(\mathbf{r})+k_{0,l}^2\int_{\Omega}\chi_l(\mathbf{r}')E_l(\mathbf{r}')G_{l,\Omega}(\mathbf{r},\mathbf{r}')\mathrm{d}\mathbf{r}'. \tag{4}$$

In these two equations, χ_l represents the contrast of complex relative permittivity at f_l, $\chi_l(\mathbf{r}) = \tilde{\varepsilon}_{r,l}(\mathbf{r}) - \tilde{\varepsilon}_{rb,l}$, and $k_{0,l}$ is the wave number of vacuum. Since χ_l changes with the frequency, as far as the inverse scattering problem is concerned, some hypothesis on the constitutive relationship of the involved media is required in order to take advantage of the frequency diversity, without neglecting the dispersive effect of background and scatterers. In several applications in the microwave domain a reliable guess is to consider an an Ohmic dispersion model with conductivity σ and neglecting the dispersion of the real part of the permittivity [*Lambert et al.*, 1998]. Then, the complex permittivity at frequency f_l is given by the following relationship:

$$\tilde{\varepsilon}_{r(b),l}(\mathbf{r})=\varepsilon_{r(b)}(\mathbf{r})-\mathrm{i}\frac{\sigma_{(b)}(\mathbf{r})}{\omega_l\varepsilon_0}. \tag{5}$$

This leads to assume as actual unknowns of the inverse scattering problem the relative permittivity ε_r and the conductivity σ, which do not depend on the frequency. On the other hand, equivalent frequency independent unknowns can be introduced also in the case of a more sophisticated model then the Ohmic one, supposed that the nature of the involved media is known.

[11] Kernels $G_{l,\Omega}$ and $G_{l,\Gamma}$ in equations (4) and (3) involve the free space Green function. The convolution structure of the integral equation in equation (4) is exploited numerically by using a fast Fourier transform (FFT) algorithm. For sake of simplicity, symbolic notations are introduced. Equations (3) and (4) are rewritten as

$$E_l^{\mathrm{d}}=\mathbf{G}_{l,\Gamma}\chi_l E_l. \tag{6}$$

$$E_l=E_l^{\mathrm{inc}}+\mathbf{G}_{l,\Omega}\chi_l E_l. \tag{7}$$

3. Inversion Scheme

[12] The aim of the inverse problem is to determine both the contrast of permittivity $\kappa = \varepsilon_r(\mathbf{r}) - \varepsilon_{rb}$ and the contrast of conductivity $\sigma(\mathbf{r}) - \sigma_b$ in Ω, such that the associated scattered field matches the measured one $\mathcal{E}^{\mathrm{mes}}$ on Γ. Many iterative methods have been developed to solve such inverse scattering problems. Starting from an initial guess, parameters of interest are adjusted gradually by minimizing a cost functional representing the discrepancy between the data and the scattered fields computed from the best available estimation of the parameters. The minimization is carried out by means of a hybrid method [*Belkebir and Tijhuis*, 2001] combining advantages of linearized methods [*Chew and Wang*, 1990], in which the field in the test domain is considered as fixed at each iteration step, and of a nonlinearized method [*Kleinman and van den Berg*, 1992], in which the field is considered as an auxiliary unknown determined together with the parameter of interest during the minimization procedure. This hybrid method is described by *Belkebir and Tijhuis* [2001] for the multistatic (multiple transmitters and multiple receivers) and time harmonic configuration.

We extend herein this method to the case of transient fields.

[13] The basic idea underlying the inversion algorithm is to build up three sequences $E_{l,n}$, ξ_n and η_n related to the total field in Ω, the real part and the imaginary part of the relative permittivity distribution. In addition, a priori information is incorporated. This information consists in stating that the real part of the relative permittivity ε_r is greater than unity (positivity of the electrical susceptibility), and the conductivity σ is positive. This is done through the transformations $\varepsilon_r(\mathbf{r}) = 1 + \xi^2(\mathbf{r})$, and $\sigma(\mathbf{r}) = \eta^2(\mathbf{r})$. The three sequences mentioned above are built up through the following recursive relations

$$E_{l,n} = E_{l,n-1} + \alpha_{l,n;v} v_{l,n} + \alpha_{l,n;w} w_{l,n}, \tag{8}$$

$$\xi_n = \xi_{n-1} + \beta_{n;\xi} d_{n;\xi}, \tag{9}$$

$$\eta_n = \eta_{n-1} + \beta_{n;\eta} d_{n;\eta}, \tag{10}$$

where $v_{l,n}$, $w_{l,n}$ are updating directions related to the field, while $d_{n;\xi}$ and $d_{n;\eta}$ are updating directions related to the electrical susceptibility and the conductivity, respectively. These updating directions are specified in Appendix A. The complex coefficients $\alpha_{l,n;v}$ and $\alpha_{l,n;w}$ and the real coefficients $\beta_{n,\xi}$ and $\beta_{n,\eta}$ are scalars obtained by minimizing at each iteration step a cost function $\mathcal{F}_n$ which writes as

$$\mathcal{F}_n(E_{l,n}; \xi_n; \eta_n) = W_\Omega . \sum_{l=1}^{L} \left\| h_{l,n}^{(1)} \right\|_\Omega^2 + W_\Gamma . \sum_{l=1}^{L} \left\| h_{l,n}^{(2)} \right\|_\Gamma^2 . \tag{11}$$

The subscripts Ω and Γ, included in the norm $\|.\|$ and later in the inner product $\langle ., . \rangle$, indicate the domain of integration. The normalization coefficients W_Ω and W_Γ are given by

$$W_\Omega = \frac{1}{\sum_{l=1}^{L} \left\| E_l^{\text{inc}} \right\|_\Omega^2}, \quad W_\Gamma = \frac{1}{\sum_{l=1}^{L} \left\| E_l^{\text{mes}} \right\|_\Omega^2}. \tag{12}$$

Functions $h_l^{(1)}$ and $h_l^{(2)}$ are residual errors computed from the observation (equation (6)) and from the state equations (equation (7)), respectively.

$$h_{l,n}^{(1)} = E_{l,n}^{\text{inc}} - E_{l,n} + \mathbf{G}_{l,\Omega} \chi_{l,n} E_{l,n}, \tag{13}$$

$$h_{l,n}^{(2)} = E_l^{\text{mes}} - \mathbf{G}_{l,\Gamma} \chi_{l,n} E_{l,n}. \tag{14}$$

[14] Once all the updating directions $v_{l,n}$, $w_{l,n}$, $d_{n,\xi}$ and $d_{n,\eta}$ are determined, $\mathcal{F}_n$ is a non linear function of $2 \times L$ complex variables ($\alpha_{l,n;v}$ and $\alpha_{l,n;w}$) and two real variables ($\beta_{n;\xi}$ and $\beta_{n;\eta}$). The minimization of $\mathcal{F}_n$ is achieved thanks to the standard Polak-Ribière conjugate gradient method [*Press et al.*, 1986]. Note that minimizing the cost function equation (11) is equivalent, via Parseval's theorem, to minimizing the same cost function where the time harmonic quantities are replaced by the associated transient ones and where the sum is over time instead of frequency.

4. Numerical Results

[15] In this section, reconstructions from synthetic data are discussed. These data are generated thanks to the forward solver described by *Peng and Tijhuis* [1993]. The incident field is generated by a wire source located at (0 m; 1.815 m) and 40 receivers collecting the transient electromagnetic field are located in vacuum, along the circle of radius 1.8 m centered at the origin. The incident pulse $\mathcal{P}(t)$ is of the form given by equation (15), with central frequency $f_0 = 2.25$ GHz and time duration $\tau = 2$ ns. The pulse shape is represented in Figure 2 in both time and frequency domains. The pulse spectrum, $P(\omega)$ is sampled into $L = 140$ frequencies, with a frequency step of 24 MHz.

$$\mathcal{P}(t) \propto \exp\left(-16 \frac{(t-\tau)^2}{\tau^2} \right) \sin(2\pi f_0 t). \tag{15}$$

4.1. Localization of Targets

[16] In the time-harmonic regime, the back-propagation technique suggested by *Kleinman and van den Berg* [1994] is often used to derive an initial guess, at least when the inverse scattering problem is addressed with the help of a domain integral formalism. In this technique, the set of receivers is used as a phase conjugation mirror, combined with a straightforward optimization to fit, as well as possible, the inverse scattering operator by the adjoint of a direct one. This allows one to localize the targets and provides a rough estimation of the contrast. In transient regime, phase conjugation mirrors become time-reversal mirrors with the same robustness and focusing properties. Further details can be found for instance in the work of *Thomas et al.* [1994]. Up to now, we have not fully generalized the aforementioned back-propagation technique to transient waves. Here, we only aim at localizing the scatterers by synthesizing the time reversed wave from the data and checking where it focuses. This information permits us to define the test domain Ω over which inversion is then performed,

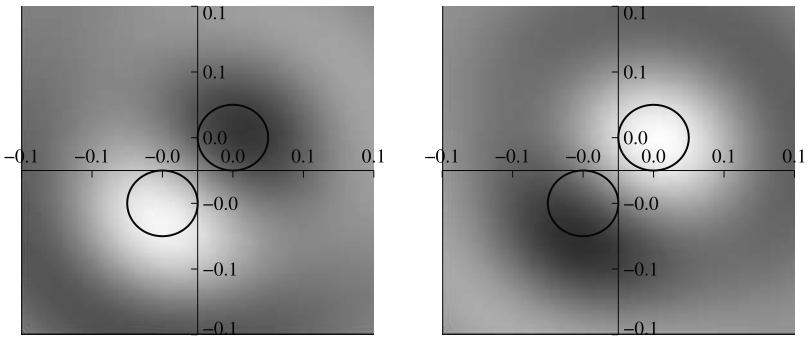

Figure 3. Modulus of the amplitude of the time-reversed wave when focusing on (a) the first target at $t = 71.6$ ns and on (b) the second one at $t = 71.75$ ns.

typically a few (central) wavelengths square centered on the bright spot.

[17] In case of multiple scatterers, if multistatic data are available, several signal processing techniques are available to separate the scatterers, for instance MUSIC, D.O.R.T. (French acronym for decomposition of the time reversal operator) [*Prada and Fink*, 1994; *Prada and Thomas*, 2003]. If the scatterers are well resolved by such methods, the inverse problem can be cast into a set of inverse problems restricted to small test areas surrounding each scatterer. However, this is only useful if their interactions are weak. Otherwise, their strong interaction enforces one to perform inversion over a connected domain that includes all the involved scatterers. In the present paper, this single connected domain is derived from the location of the maxima of the amplitude of the time-reversed wave, which focuses on the various scatterers at various times with an amplitude proportional to their contribution to the scattered field. An example is given in Figure 3 for two small scatterers located in the vicinity of the origin. Focusing occurs at $t = 71.60$ ns and $t = 71.75$ ns respectively, with maxima 15 cm away from each other. Therefore, in the following, the test domain Ω is reduced to a square box of size (0.2×0.2) m^2 centered at the origin and subdivided into 64×64 square cells.

4.2. Frequency Hopping and Time Reversal Approaches

[18] In this section the problem of reconstructing targets from their transient scattered fields is addressed. We compare herein, through the case of a single target, inversions using the frequency-hopping approach and the transient inversion method as described in the previous section. Particular attention is devoted to the robustness of both the aforementioned strategies against unavailable measurement noise.

[19] Let us consider a single homogeneous dielectric target in vacuum ($\varepsilon_r = 2$, $\sigma = \sigma_b = 0$). In the frequency-hopping approach, the inversion algorithm is first performed at low frequency, and the result is then used as initial guess at higher frequencies. This way, 140 inverse harmonic problems have been solved successively. The initial guess at the lowest available frequency is derived from the back-propagation procedure with $L = 1$. For each time-harmonic inversion, the iterative process was ended at the 20th iteration step. We did not notice any significant change when continuing iterating. Results using this strategy with noiseless data are presented in Figure 4a where only the real part of the relative permittivity is plotted, because the reconstructed conductivity distribution is almost null in the investigated domain. In this paper maps of the reconstructed conductivity profiles are not presented when, according to the actual one, the reconstructed conductivity value is negligible.

[20] In the second strategy, transient inversion, the entire spectrum of the scattered field is considered, each of the 140 harmonic components being weighted by the power spectrum of the incident pulse $P(\omega)$. In this case, a single inverse scattering problem is solved. As above, the initial guess is deduced from the back-propagation procedure, with however a larger amount of data. Result of the reconstruction with noiseless data, corresponding to the 200th iteration step, is presented in Figure 4b.

[21] Comparing Figures 4a and 4b leads to the conclusion that both approaches provide similar result from noiseless data. In both cases, the target is detected and well located. However, some differences appear on the illuminated side: the frequency-hopping approach presents in the area of the illuminated side an overestimated relative permittivity as compared to the estimated relative permittivity obtained with the transient

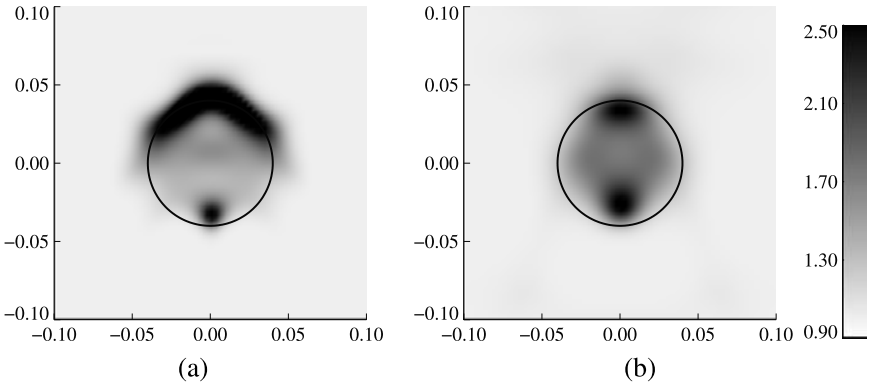

Figure 4. Reconstructed permittivity of a single cylinder from noiseless data. (a) Using a frequency-hopping approach in the frequency band [0.8–4.2] GHz with a frequency step of 24 MHz. (b) Using the transient inversion algorithm as described in section 3 with an incident pulse of central frequency f_0 = 2.25 GHz and time duration τ = 2 ns. The black circle represents the actual boundary of the target.

inversion in the same area. Clearly, the inversions are not precise. Nevertheless, with both approaches, valuable information is obtained that could suffice in many applications.

[22] Now, let us study the robustness of the inversion algorithms against noise. To this end, a random perturbation is added to the real and imaginary parts of the harmonic components of the scattered field according to

$$\Re e\left[E_l^{\mathrm{d;noise}}(\mathbf{r})\right] = \Re e\left[E_l^{\mathrm{d}}(\mathbf{r})\right] + b\ \phi_l\left(E_l^{\mathrm{R;max}} - E_l^{\mathrm{R;min}}\right), \tag{16}$$

$$\Im m\left[E_l^{\mathrm{d;noise}}(\mathbf{r})\right] = \Im m\left[E_l^{\mathrm{d}}(\mathbf{r})\right] + b\ \Phi_l\left(E_l^{\mathrm{I;max}} - E_l^{\mathrm{I;min}}\right), \tag{17}$$

where b is a number that monitors the level of noise and ϕ_l and Φ_l are random numbers uniformly distributed between -1 and 1. $E_l^{\mathrm{R;max}}$ and $E_l^{\mathrm{R;min}}$ denotes the maximum and the minimum of the real part of the scattered field, respectively, for the frequency l and for all receivers. $E_l^{\mathrm{I;max}}$ and $E_l^{\mathrm{I;min}}$ denotes the maximum and the minimum of the imaginary part of the scattered field, respectively, for the frequency l and for all receivers.

[23] Reconstructions from noisy data, with b = 10%, are presented in Figure 5 where the two aforementioned approaches are compared. Figure 5a clearly shows that the frequency hopping does not provide any reliable information regarding the target under test. Neither the geometry nor the localization of the target is well determined. This is not the case when the transient inversion is performed. The result is shown in Figure 5b, and it is similar to the result given in Figure 4b obtained by processing noiseless data. This numerical experiment shows that the transient inversion is more robust against noise than the frequency-hopping approach. From now on, only the transient inversion is considered.

4.3. Resolution and Incident Field Features

[24] In this section, the focus is on the influence of the characteristics (central frequency f_0 and time duration τ) of the incident pulse on the the reconstruction capabilities of the transient inversion strategy. The scattering system is now composed of two cylinders one near to the other one. In this case, our aim is to separate the cylinders as well as to estimate their constitutive features.

[25] Let us consider two small, identical, homogeneous, circular dielectric cylinders with radius a = 0.02 m and permittivity ε_r = 2. The centers of the cylinders are at (0.02 m; 0.02 m) and (−0.02 m; −0.02 m). The incident pulse is of the same type as previously (equation (15)) with central frequency f_0 = 2.25 GHz and time duration τ = 2 ns. Its spectrum is still sampled into L = 140 frequencies, with a frequency step of 24 MHz.

[26] As a reference, the reconstructed permittivity profile from noiseless data is plotted in Figure 6a, whereas the reconstructed profile from noisy data (b = 10%) is plotted in Figure 6b. It is to be noticed that the two cylinders are separated by a distance of about $\frac{\lambda_0}{8}$ (λ_0 being the wavelength at the central frequency f_0 and the separating distance being defined as the distance between the boundaries of the cylinders). The reconstructed objects are clearly separated, and remarkably the presence of such a noise does not alter the power of

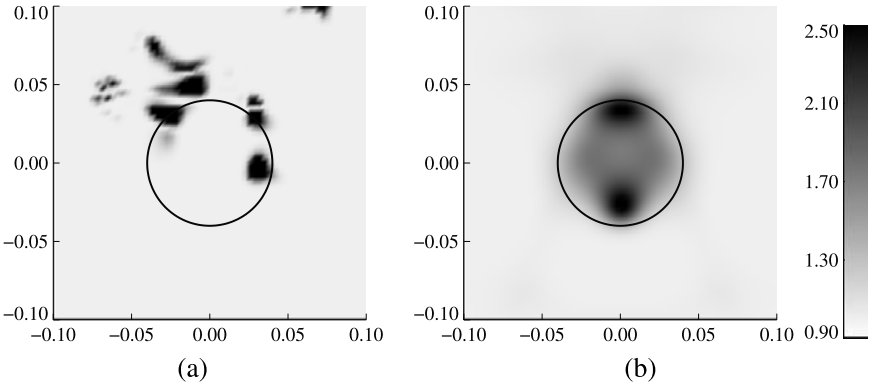

Figure 5. Same as in Figure 4 but with noisy data (b = 10%).

resolution. This "super-resolution" (better than the Rayleigh criterion) may be due to the fact that multiple scattering effects are taken into account in the inversion algorithm [*Chen and Chew*, 1998].

[27] However, it should also be noticed that the retrieved value of the permittivity is overestimated. Indeed, as shown in Figures 6c and 6d, the maximum value of the reconstructed permittivity is about 2.5 instead of 2.

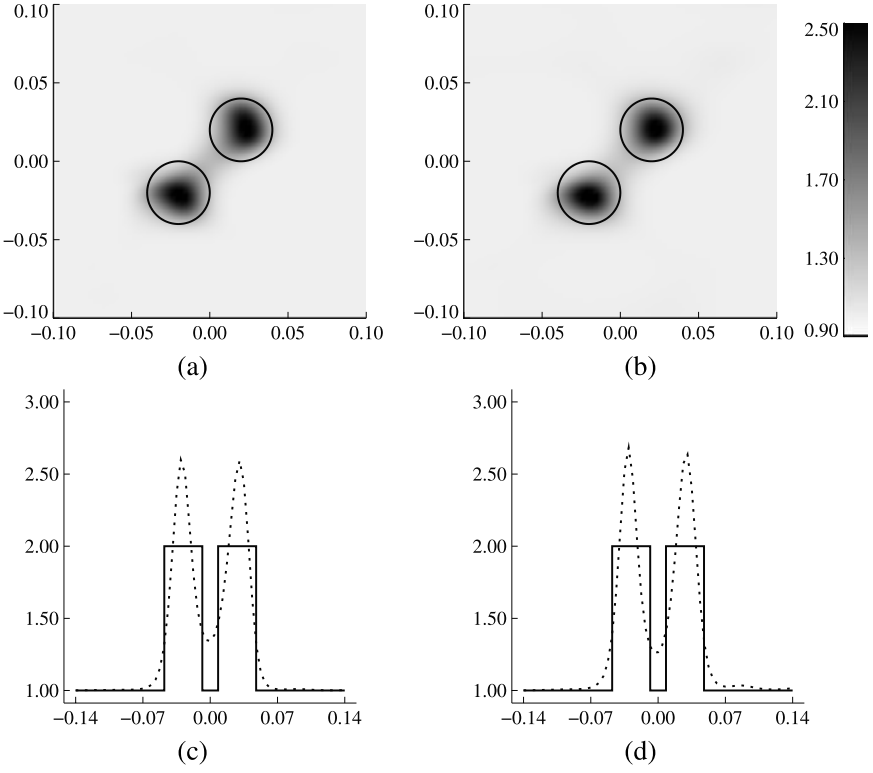

Figure 6. Reconstructed permittivity distribution using the transient inversion method. Targets under test are twin circular cylinders located along the antidiagonal of the test domain Ω. Radius of each cylinder is a = 0.02 m. Coordinates of the centers of the cylinders are (0.02 m, 0.02 m) and (−0.02 m, −0.02 m). Characteristics of the incident pulse are the same as previously. (a) Noiseless data; (b) noisy data (b = 10%). (c and d) Present comparisons between the reconstructed profile (dashed line) and the actual one (full line) along the antidiagonal of the test domain Ω, corresponding to Figures 6a and 6b, respectively.

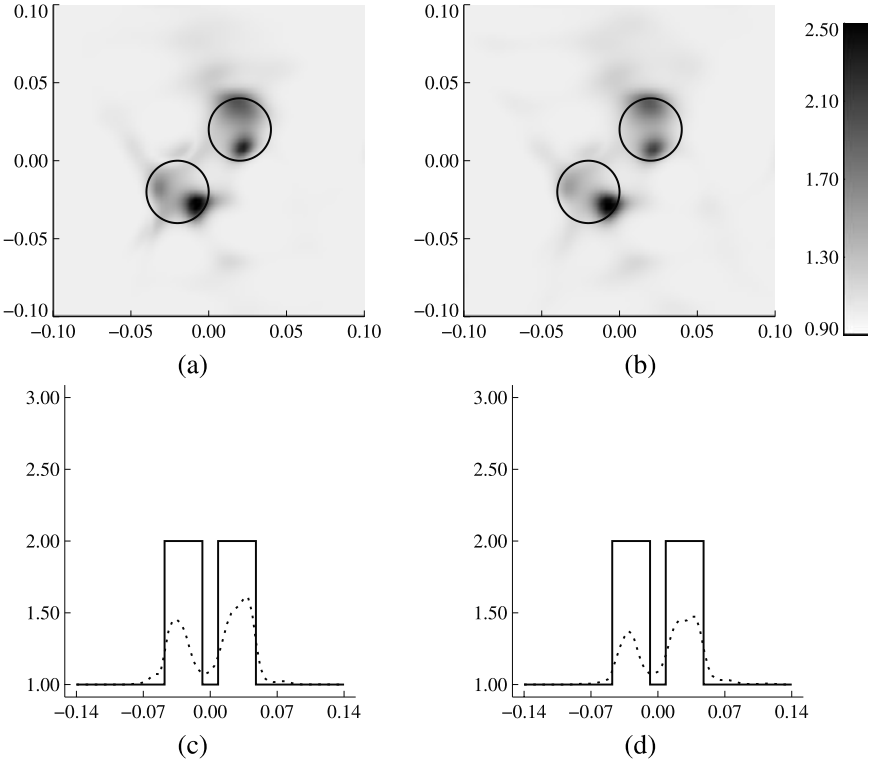

Figure 7. Same as in Figure 6 but using an incident pulse of central frequency f_0 = 4.25 GHz instead of f_0 = 2.25 GHz.

Therefore, strategies to improve the characterization of the cylinders are also investigated. In a recent work [*Dubois et al.*, 2006], improvement of the accuracy from stepped-frequency data is suggested. It consists in applying a ''central-frequency-hopping approach,'' i.e., illuminating the target with pulses of different central frequencies and performing inversions sequentially, from data corresponding to low central frequencies up to higher ones and using the previous final result as initial guess. This strategy has been successfully applied to experimental data and is not repeated here.

[28] In the present paper, we consider a single pulse illumination and tune the two parameters, the central frequency f_0 and the time duration τ of the incident pulse. In principle, the resolution should be improved at higher frequencies. Let us consider the same twin cylinders as previously, illuminated by a pulse with higher central frequency, f_0 = 4.25 GHz, and same time duration τ = 2 ns. The results of the inversion from noiseless and noisy data are presented in Figure 7, the initial guess being still deduced from a back-propagation procedure. As compared to Figure 6, these results are not satisfactory. The inversion scheme seems to be trapped in a local minimum, although the twin cylinders are still resolved.

[29] We now choose to tune the time duration of the incident pulse also. The time duration is reduced, τ = 1 ns, and the central frequency is shifted to f_0 = 3.25 GHz, such that the spectrum of this pulse covers the frequency ranges of the two previous pulses (f_0 = 2.25 GHz, τ = 2 ns and f_0 = 4.25, τ = 2 ns), with the hope that this pulse takes advantage of high frequencies in terms of resolution and of low frequencies in terms of dynamic range of convergence of the iterative inverse scheme. The sampling of the spectrum of the incident pulse remains the same (L = 280). Results of the inversion are reported in Figure 8 for both noiseless and noisy data. One can observe that not only the cylinders are as well separated as in Figure 6 but also a better characterization of the constitutive materials is achieved. This is emphasized in Figures 8c and 8d.

4.4. Reconstruction Capabilities

[30] In the previous section we have shown how the reconstruction capabilities of the transient inversion approach may be improved by properly setting the parameters of the incident pulse. In order to verify further on the achievable performances inhomogeneous objects having a not negligible conductivity value are

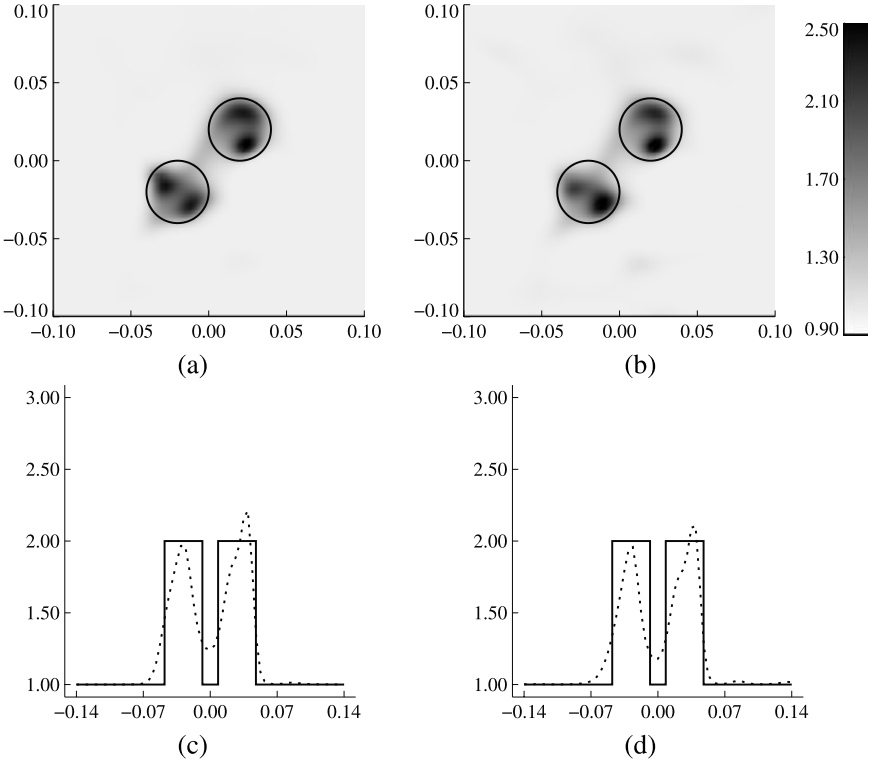

Figure 8. Same as in Figure 6 but using an incident pulse of central frequency f_0 = 3.25 GHz and time duration τ = 1 ns.

now considered. Synthetic data have been generated by considering the previously described measurement configuration and have been corrupted by noise as stated in equations (16) and (17). The incident impulse has central frequency f_0 equal to 3.25 GHz and time duration τ = 1 ns; its spectrum has been sampled by means of L = 192 samples.

[31] As first example let us consider the case of two homogeneous cylinder having radius r = 0.015 m but different electrical characteristics. In particular, the cylinder with center in (−0.05 m; −0.03 m) has relative permittivity ε_{r1} = 2.3 and null conductivity, while that one centered in (0.05 m; −0.03 m) has relative permittivity ε_{r2} = 2 and conductivity σ_2 = 0.1 S/m. The 50th estimate of the parameter of interest is plotted in Figure 9 while the evolution of the minimized cost function $\mathcal{F}_n$ as a function of iteration is presented in Figure 10. The reconstructed permittivity profile is given in Figure 9a while the conductivity one is given in Figure 9b. As in the previous examples, the black circles represent the actual boundaries of the targets. Comparisons between the actual profiles and the reconstructed ones along a direction parallel to the x axis are reported in Figures 9c and 9d. All these figures show that the geometrical as well as constitutive features of both the scatterers are well identified and allow us to state that only the right object is purely dielectric. On the other hand, while the permittivity values of both the targets are retrieved with satisfactory accuracy (ε_{r1} = 2.5, ε_{r2} = 1.8), the conductivity value of the left objects is more than twice of the actual one (σ_2 = 0.24 S/m). Moreover, the location of the right cylinder is perfectly retrieved while the left object appears a little bit shifted. As the reconstructed profiles of permittivity and conductivity appear to be shifted in opposite directions, the correct location may be obtained by considering an average of the two retrieved positions. The mismatch error between the reconstructed permittivity profile and the actual one is err_ε = 0.0099, while at the central frequency the mismatch between the reconstructed contrast function and the actual one is err_χ = 0.0148. The mismatch error mentioned above err_ε and err_χ are defined as follows:

$$\mathrm{err}_\varepsilon = \frac{\|\varepsilon_{\mathrm{recons}} - \varepsilon_{\mathrm{actual}}\|_\Omega^2}{\|\varepsilon_{\mathrm{actual}}\|_\Omega^2}, \tag{18}$$

$$\mathrm{err}_\chi = \frac{\|\chi_{\mathrm{recons}} - \chi_{\mathrm{actual}}\|_\Omega^2}{\|\chi_{\mathrm{actual}}\|_\Omega^2}, \tag{19}$$

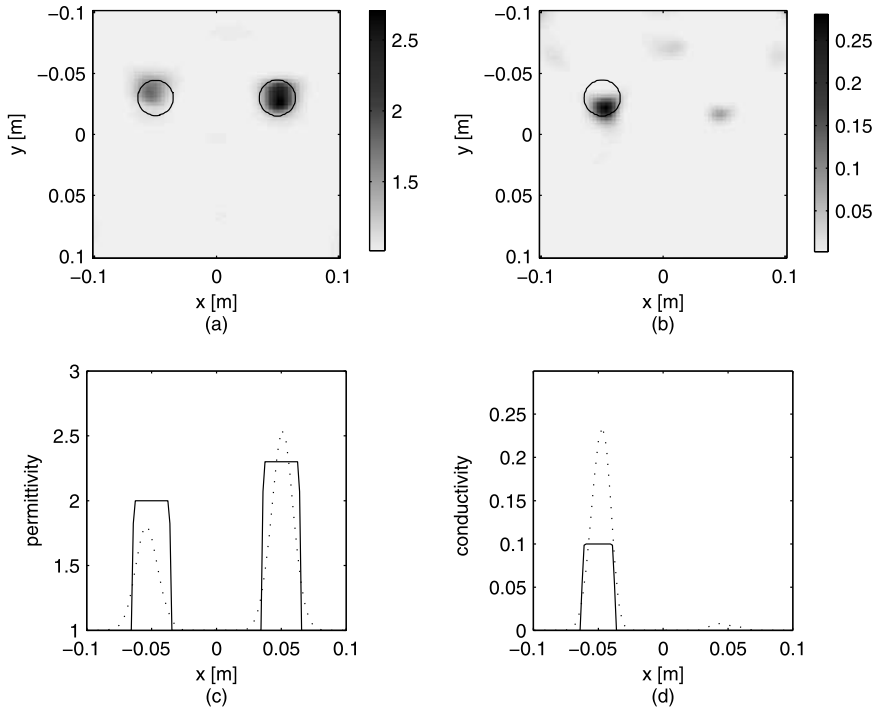

Figure 9. Reconstruction of two inhomogeneous cylinders using the transient inversion method. (a) Permittivity profile, (b) conductivity profile, (c) comparison of the actual permittivity profile (full line) and the reconstructed one (dashed line) along a direction parallel to the x axis, and (d) comparison of the actual conductivity profile (full line) and the reconstructed one (dashed line) along a direction parallel to the x axis.

where $\varepsilon_{\text{recons}}$ and $\varepsilon_{\text{actual}}$ denote the reconstructed permittivity distribution and the actual permittivity profile, respectively; while χ_{recons} and χ_{actual} denote the reconstructed contrast distribution and the actual contrast profile, respectively.

[32] As a second example let us consider the case of an inhomogeneous object made of two cylinders having different geometrical and electrical features and one close to the other one. The smaller cylinder has radius r_1 = 0.015m, relative permittivity ε_{r1} = 2.5 and conductivity σ_1 = 0.1 S/m; the larger cylinder is purely dielectric (ε_{r2} = 2, σ_2 = 0 S/m) and its radius is r_2 = 0.03 m. As the Shannon's theorem may lead to consider a larger number of frequencies then that required to collect all the independent data [*Bucci et al.*, 2000], a reduced number of frequencies has been considered in this example. In order to choose a value of L such to possibly avoid redundant frequencies without loosing available independent data, we have taken into account, for a given reference scenario, an upper bound of the essential dimension of the data space. This can be achieved through the Singular Value Decomposition (SVD) of the radiation operator [*Bucci and Isernia*, 1997]. Hence, we have computed the SVD of the multistatic multifrequency operator, which relates the

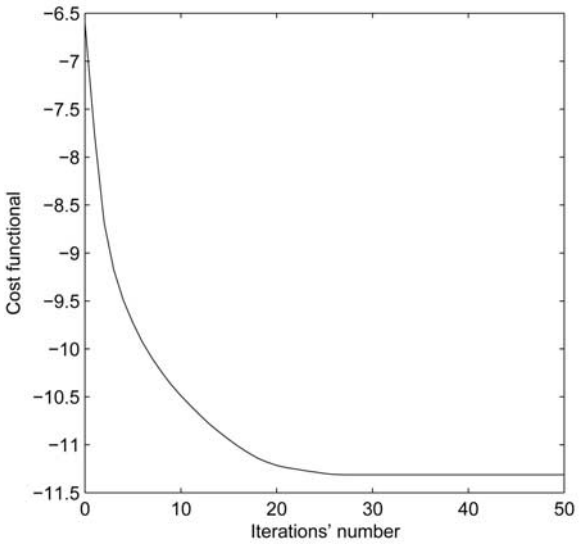

Figure 10. Evolution of the cost function $\mathcal{F}_n$ as a function of iteration. This cost function corresponds to the reconstruction of Figure 9.

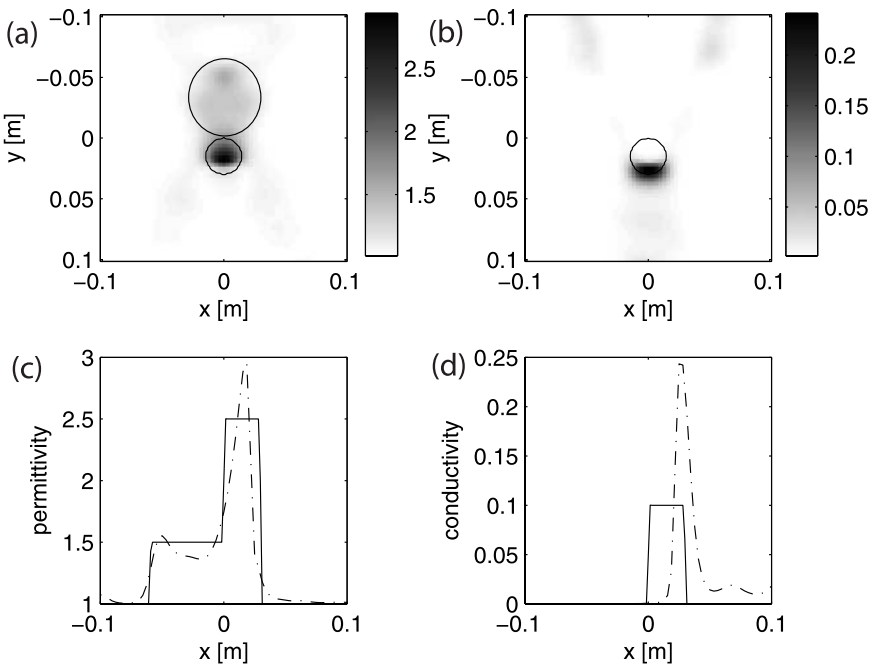

Figure 11. Reconstruction of two inhomogeneous cylinders using the transient inversion method with a reduced number of frequencies. (a) Permittivity profile, (b) conductivity profile, (c) comparison of the actual permittivity profile (full line) and the reconstructed one (dashed line) along a direction parallel to the x axis, and (d) comparison of the actual conductivity profile (full line) and the reconstructed one (dashed line) along a direction parallel to the x axis.

induced current in the investigating domain Ω by the considered incident pulse to the scattered field measured along the line Γ, for a fixed number of measurement points ($N_m = 40$) and increased the number of frequencies. By plotting the behavior of the singular values obtained for different values of L, we observed that, whatever the fixed accuracy is, the number of significant singular values does not change when L is larger than 48. Therefore, $L = 48$ has been chosen as a suitable number to uniformly sample the spectrum of the incident pulse. The 50th estimate of the parameter of interest is plotted in Figure 11 while the evolution of the minimized cost function $\mathcal{F}_n$ as a function of iteration is presented in Figure 12. The reconstructed permittivity and conductivity profiles are in Figures 11a and 11b, respectively. Figures 11a and 11b show that the inhomogeneous nature of the target is clearly identified as well as its location and its conducting component. Moreover, the permittivity and conductivity values of the larger cylinder are accurately retrieved while those of the smaller one are overestimated ($\varepsilon_{r1} = 2.9, \sigma_1 = 0.24$, S/m). This is emphasized by the comparisons between actual profiles and reconstructed ones along the illumination direction, i.e., x = 0, which are given in Figures 11c and 11d. The mismatch error between the reconstructed permittivity profile and the

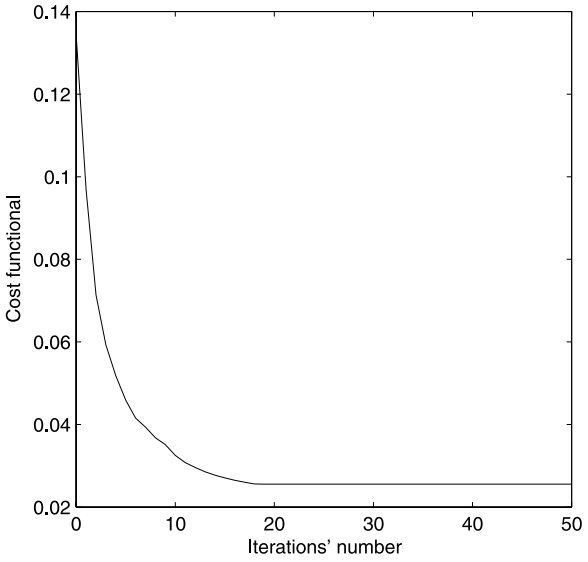

Figure 12. Evolution of the cost function $\mathcal{F}_n$ as a function of iteration. This cost function corresponds to the reconstruction of Figure 11.

actual one is $\mathrm{err}_\varepsilon = 0.0105$, while at the central frequency the mismatch between the reconstructed contrast function and the actual one is $\mathrm{err}_\chi = 0.0182$. Furthermore, the same reconstruction accuracy is achieved, when the number of frequencies is fixed according to the Shannon's rule ($L = 192$). Indeed, for this cas ($L = 192$) the mismatch errors are $\mathrm{err}_\varepsilon = 0.0101$ and $\mathrm{err}_\chi = 0.0179$. Such a result corroborates that, by uniformly sampling the spectrum of the incident pulse by means of $L = 48$ samples, one does not loose significant information with respect to the target under test contained in the data. Hence, the computational burden is reduced without affecting the effectiveness of the reconstruction strategy. Finally, it is worth to note that in both the examples 30 iterations were sufficient to reach the convergence.

5. Conclusion

[33] An iterative algorithm has been developed to reconstruct targets embedded in an infinite and homogeneous background medium, from transient scattering data. The inverse scattering problem is stated in the frequency domain, thanks to a temporal Fourier transform, rather than directly in the time domain. The suggested iterative approach for solving the inverse problem considers the entire spectrum at once through a single iterative process. The robustness of the inverse scheme against noise has been analyzed and it has been shown that the transient inversion is very stable. We also investigated enhancement of the resolution by tuning solely parameters of the incident pulse (central frequency and time duration). The reconstruction capabilities of the proposed strategy was satisfactory both in the case of purely dielectric targets and of dielectric cylinders whose conductivity is not negligible.

Appendix A: Updating Directions

[34] In this section is presented the choice of the updating directions for both contrast and field used in the inverse algorithm described in section 3. The two updating directions $d_{n;\xi}$ and $d_{n;\eta}$ associated with the real and imaginary parts of the contrast are given by the standard Polak-Ribière conjugate gradient directions

$$d_{n;\xi} = g_{n;\xi} + \gamma_{n;\xi} d_{n-1;\xi} \text{ with } \gamma_{n;\xi} = \frac{\left\langle g_{n;\xi} | g_{n;\xi} - g_{n-1;\xi} \right\rangle_\Omega}{\|g_{n-1;\xi}\|_\Omega^2}, \tag{A1}$$

$$d_{n;\eta} = g_{n;\eta} + \gamma_{n;\eta} d_{n-1;\eta} \text{ with } \gamma_{n;\eta} = \frac{\left\langle g_{n;\eta} | g_{n;\eta} - g_{n-1;\eta} \right\rangle_\Omega}{\|g_{n-1;\eta}\|_\Omega^2}, \tag{A2}$$

where $g_{n;\xi}$ and $g_{n;\eta}$ are the gradients of the cost function $\mathcal{F}_n$ with respect to ξ and η assuming that the total field in Ω does not change. These gradients are given by

$$g_{n;\xi} = 2\xi_{n-1} \Re e\left\{ W_\Omega \sum_{l=1}^{L} E^\star_{l,n-1} \mathbf{G}^\dagger_{l,\Omega} h^{(1)}_{l,n-1} + W_\Gamma \sum_{l=1}^{L} E^\star_{l,n-1} \mathbf{G}^\dagger_{l,\Gamma} h^{(2)}_{l,n-1} \right\}, \tag{A3}$$

$$g_{n;\eta} = \frac{-2}{\omega \varepsilon_0} \eta_{n-1} \Im m\left\{ W_\Omega \sum_{l=1}^{L} E^\star_{l,n-1} \mathbf{G}^\dagger_{l,\Omega} h^{(1)}_{l,n-1} + W_\Gamma \sum_{l=1}^{L} E^\star_{l,n-1} \mathbf{G}^\dagger_{l,\Gamma} h^{(2)}_{l,n-1} \right\}. \tag{A4}$$

where $\star$ refers to the complex conjugation. $\mathbf{G}^\dagger_{l,\Omega}$ and $\mathbf{G}^\dagger_{l,\Gamma}$ are the adjoint operators of $\mathbf{G}_{l,\Omega}$ and $\mathbf{G}_{l,\Gamma}$, respectively.

[35] The field updating direction $v_{l,n}$ is similar to those chosen for ξ_n and η_n, and it is given by

$$v_{l,n} = g_{l,n;E_l} + \gamma_{l,n;E_l} v_{l,n-1} \text{ with } \gamma_{l,n;E_l} = \frac{\left\langle g_{l,n;E_l} | g_{l,n;E_l} - g_{l,n-1;E_l} \right\rangle_\Omega}{\|g_{l,n-1;E_l}\|_\Omega^2}, \tag{A5}$$

where $g_{l,n;El}$ corresponds to the gradient of the cost function $\mathcal{F}_n$ with respect to E_l, assuming that ξ and η do not change. It is given by

$$g_{l,n;E_l} = W_\Omega \left\{ \chi^\star_{l,n-1} \mathbf{G}^\dagger_{l,\Omega} h^{(1)}_{l,n-1} - h^{(1)}_{l,n-1} \right\} - W_\Gamma \chi^\star_{l,n-1} \mathbf{G}^\dagger_{l,\Gamma} h^{(2)}_{l,n-1}. \tag{A6}$$

[36] The second field updating direction $w_{l,n}$ is given by

$$w_{l,n} = \tilde{E}_{l,n-1} - E_{l,n-1}; \tilde{E}_{l,n-1} = \left[1 - \mathbf{G}_{l,\Omega} \chi_{l,n-1}\right]^{-1} E^{\mathrm{inc}}_l. \tag{A7}$$

[37] The function $\tilde{E}_{l,n}$ corresponds to the total field computed from the field equation (equation (7)) with the contrast $\chi_{l,n-1}$. It is the solution of the forward problem with the contrast $\chi_{l,n-1}$. In practice, the computation of $\tilde{E}_{l,n-1}$ uses a fast forward solver. Details of this forward solver are given by *Peng and Tijhuis* [1993]. The initial guess of the iterative inversion scheme is given by the back-propagation procedure.

References

Belkebir, K., and A. G. Tijhuis (2001), Modified[2] gradient method and modified Born method for solving a two-dimensional inverse scattering problem, *Inverse Probl.*, *17*(6), 1671–1688.

Bucci, O. M., and T. Isernia (1997), Electromagnetic inverse scattering retrievable information and measurement strategies, *Radio Sci.*, *32*, 2123–2138.

Bucci, O. M., L. Crocco, T. Isernia, and V. Pascazio (2000), Inverse scattering problems with multifrequency data: Reconstruction capabilities and solution strategies, *IEEE Trans. Geosci. Remote Sens.*, *38*(4), 1749–1756.

Catapano, I., L. Crocco, R. Persico, M. Pieraccini, and F. Soldovieri (2006), Linear and nonlinear microwave tomography approaches for subsurface prospecting: Validation on real data, *IEEE Antennas Wireless Propag. Lett.*, *5*, 49–53, doi:10.1109/LAWP.2006.870363.

Chen, F. C., and W. C. Chew (1998), Experimental verification of super resolution in nonlinear inverse scattering, *Appl. Phys. Lett.*, *72*(23), 3080–3082.

Chew, W. C., and J. H. Lin (1995), A frequency-hopping approach for microwave imaging of large inhomogeneous bodies, *IEEE Microwave Guided Wave Lett.*, *5*(12), 439–441.

Chew, W. C., and Y. M. Wang (1990), Reconstruction of two-dimensional permittivity distribution using distorted Born iterative method, *IEEE Trans. Med. Imaging*, *9*, 218–225.

Dubois, A., J. M. Geffrin, K. Belkebir, and M. Saillard (2006), Imaging of dielectric cylinders from experimental stepped-frequency data, *Appl. Phys. Lett.*, *88*(16), 164,104.

Kleinman, R. E., and P. M. van den Berg (1992), A modified gradient method for two-dimensional problems in tomography, *J. Comput. Appl. Math.*, *42*, 17–35.

Kleinman, R. E., and P. M. van den Berg (1994), Two-dimensional location and shape reconstruction, *Radio Sci.*, *29*(4), 1157–1169.

Lambert, M., D. Lesselier, and B. J. Kooij (1998), The retrieval of a buried cylindrical obstacle by a constrained modified gradient method in the H-polarization case and for Maxwellian materials, *Inverse Probl.*, *14*(5), 1265–1283.

Moghaddam, M., and W. C. Chew (1992), Nonlinear two-dimensional velocity profile inversion using time domain data, *IEEE Trans. Geosci. Remote Sens.*, *30*, 147–156.

Moghaddam, M., and W. C. Chew (1993), Study of some practical issues in inversion with the Born iterative method using time-domain data, *IEEE Trans. Antennas Propag.*, *41*, 177–184.

Peng, Z. Q., and A. G. Tijhuis (1993), Transient scattering by a lossy dielectric cylinder: marching-on-in-frequency approach, *J. Electron. Waves Appl.*, *7*(5), 739–763.

Prada, C., and M. Fink (1994), Eigenmodes of the time reversal operator: A solution to selective focusing in multiple-target media, *Wave Motion*, *20*, 151–163.

Prada, C., and J. L. Thomas (2003), Experimental subwavelength localization of scatterers by decomposition of the time reversal operator interpreted as a covariance matrix, *J. Acoust. Soc. Am.*, *114*(1), 235–243, doi:10.1121/1.1568759.

Press, W. H., B. P. Flannery, S. A. Teukolski, and W. T. Vetterling (1986), *Numerical Recipes: The Art of Scientific Computing*, Cambridge Univ. Press, New York.

Thomas, J. L., P. Roux, and M. Fink (1994), Inverse scattering analysis with an acoustic time-reversal mirror, *Phys. Rev. Lett.*, *72*(5), 637–640.

Tijhuis, A. G. (1981), Iterative determination of permittivity and conductivity profiles of a dielectric slab in the time domain, *IEEE Trans. Antennas Propag.*, *29*(2), 239–245.

Tijhuis, A. G., K. Belkebir, A. C. S. Litman, and B. P. de Hon (2001a), Theoretical and computational aspects of 2-D inverse profiling, *IEEE Trans. Geosci. Remote Sens.*, *39*(6), 1316–1330.

Tijhuis, A. G., K. Belkebir, A. C. S. Litman, and B. P. de Hon (2001b), Multiple-frequency distorted-wave Born approach to 2D inverse profiling, *Inverse Probl.*, *17*(6), 1635–1644.

Weedon, W., and W. C. Chew (1993), Time-domain inverse scattering using the local shape function (LFS) method, *Inverse Probl.*, *9*, 551–564.

K. Belkebir, Institut Fresnel, UMR6133, Universités d'Aix-Marseille I and III, CNRS, Campus de Saint Jérôme, case 162, F-13397 Marseille CEDEX, France. (kamal.belkebir@fresnel.fr)

I. Catapano, Institute for Electromagnetic Sensing of the Environment, IREA-CNR, I-80124 Napoli, Italy.

A. Dubois, LIST, CEA, F-91191 Gif-sur-Yvette CEDEX, France.

M. Saillard, LSEET, UMR6017, Université de Sud Toulon-Var, CNRS, F-83957 La Garde CEDEX, France.